Materials Research. 2023; 26:e20230235
DOI: https://doi.org/10.1590/1980-5373-MR-2023-0235

Influence of Substrate Temperature on Microstructure of Zirconium Silicon Nitride Thin Films Deposited by Reactive Magnetron Sputtering

F.S. Oliveira[a], I.L. Dias[a], P.L.L. Araújo[a], D.A. Ramirez[a], P.C. Silva Neto[b], R. Hübler[c], F.M.T. Mendes[d], I.Z. Damasceno[e], E.K. Tentardini[a]*

[a]*Universidade Federal de Sergipe, Av. Marechal Rondon, S/N, São Cristóvão, SE, Brasil.*
[b]*Universidade Federal da Bahia, Escola Politécnica, Rua Prof. Aristides Novis, nº 02, Federação, Salvador, BA, Brasil.*
[c]*Pontifícia Universidade Católica do Rio Grande do Sul, Av. Ipiranga, 6681, Porto Alegre, RS, Brasil.*
[d]*Instituto Nacional de Tecnologia, Av. Venezuela, 82, Rio de Janeiro, RJ, Brasil.*
[e]*Universidade Federal do Rio Grande do Norte, Centro de Ciências Exatas e da Terra, Av. Senador Salgado Filho, 3000, Natal, RN, Brasil.*

Received: May 10, 2023; Revised: August 03, 2023; Accepted: September 14, 2023

Zr-Si-N thin films were co-deposited by reactive magnetron sputtering to verify the influence of silicon content (1.6 and 8.0 at. % Si) and substrate temperature (room temperature and heated to 973 K) on structure, morphology, chemical bonds and hardness. GAXRD shows a change in grain orientation from (111) to (200) due substrate heating for sample $Zr_{0.984}Si_{0.016}N$, furthermore, it was not possible to identify any silicon compounds in all deposited samples. SEM-FEG images show greater roughness and surface clusters for sample $Zr_{0.920}Si_{0.080}N$ due to the heat applied on the substrate, with Si_3N_4 decomposition, influencing thin film hardness. XPS analyses of Si 2p photoelectronic region shows only Si_3N_4 presence in all samples, proving, in conjunction with other characterization results, the non-formation of substitutional or interstitial solid solution, regardless of substrate heating or silicon content added to ZrN matrix.

Keywords: *thin films, solid solution, substrate heating, ZrN, Si_3N_4, reactive magnetron sputtering.*

1. Introduction

Zirconium silicon nitride thin films (Zr-Si-N) have shown promising results when used in diverse industrial applications due to higher hardness and oxidation resistance at high temperatures when compared to pure zirconium nitride (ZrN)[1-3].

As a consensus in literature, amorphous silicon nitride (Si_3N_4) is formed around ZrN grains when silicon content is above 2 at. %. From 6 at. % Si and beyond, the increasing amount of this amorphous phase is responsible for decreasing thin film hardness and wear resistance[4-7].

A recent investigation[8] has shown that, even at low concentration (1.6 at. %), silicon atoms are incorporated in ZrN structure as Si_3N_4 amorphous phase, not forming a substitutional or interstitial solid solution with ZrN, as frequently reported in previous works[5,9,10].

In parallel, it is well understood that substrate heating is a parameter that may enable a Zr-Si-N solid solution[2,11]. However, reports regarding the influence of substrate heating on chemical bonds, phases, structure and hardness of zirconium silicon nitride thin films are scarce in literature.

Therefore, the present work aims to investigate the influence of substrate temperature on the microstructure and hardness of zirconium silicon nitride thin films. For this purpose, Zr-Si-N thin films with low and high silicon concentrations (1.6 and 8.0 at. %) were deposited by reactive magnetron sputtering, at room temperature and heated to 973 K.

Deposited thin films were characterized by Rutherford backscattering spectroscopy (RBS), grazing angle X-ray diffraction (GAXRD), scanning electron microscopy (SEM-FEG), X-Ray Photoelectron Spectroscopy (XPS) and nanohardness tests.

2. Materials and Methods

Zirconium silicon nitride thin films with 1.6 at. % and 8.0 at. % Si were co-deposited by reactive magnetron sputtering, using AJA Orion 5-HV sputtering system. Two targets were simultaneously used for coatings deposition, zirconium and silicon, with purities of 99.8% and 99.9%, respectively. Polyethylene and (100) oriented silicon wafers were utilized as substrates, depending on the characterization techniques used. All substrates were cleaned in acetone using an ultrasonic bath for 15 minutes, prior to being inserted in the vacuum chamber.

For thin films deposition, all parameters were kept constant, with exception of power applied to Si target and substrate temperature: base pressure: 3×10^{-5} Pa, working pressure: 4×10^{-1} Pa, Zr target power: 120 W, Si target power: $Zr_{0.984}Si_{0.016}$ N: 15 W and $Zr_{0.920}Si_{0.080}N$: 90 W, Ar–N_2 flows: 19–2 sccm, substrate temperature: room temperature (RT) and 973 K. The substrate heating was carried out by a 1000 W tungsten halogen lamp located behind the sample holder.

*e-mail: fabiogabrieloliveira211@gmail.com.br

Deposition times were determined based on each characterization technique to be utilized, 12 minutes for RBS samples and 60 minutes for GAXRD, SEM-FEG, XPS and nanohardness samples. Thicknesses of approximately 80 and 350 nm were obtained, respectively.

RBS analyses were performed in a 3 MV Tandetron equipment, using He^{++} particles accelerated with 2 MeV and a silicon detector at 165°. Elemental composition was estimated using RUMP software. GAXRD tests were executed using a Shimadzu XRD-600 equipment with Cu-Kα radiation (λ=1.54 Å), grazing angle incidence of 1°, step size of 0.02° and 2°/min scan speed.

Carl Zeiss Auriga 40 scanning electron microscope with field emission gun (SEM-FEG) equipment was used for cross-section analyses. X-ray photoelectron spectra (XPS) were recorded using a hemispherical spectrometer PHOIBOS 150- SPECS, equipped with X-ray Gun (XR-50) with an Al Kα source (soft X-ray source at 1486.6 eV, which is non-monochromatic). The anode was operated at 10 W (10 kV, 10 mA) and the analyzer was used at a constant pass energy of 50 eV for survey spectra and 20 eV for selected regions. The binding energy shifts due to surface charging were corrected using the C 1s level at 284.6 eV, as an internal standard. The spectra were Shirley background-subtracted across the energy region and fitted using CasaXPS Version 2.3.15.

Nanoindentation tests were performed by Fisherscope HV 100 equipment with Berkovich indenter. In order to minimize the substrate influence in resulting values, a load of 10 mN was applied. Hardness values were calculated according to ISO 14577 standard.

3. Results and Discussion

3.1. RBS

Initially, several zirconium nitride thin films with varying silicon content were deposited by exclusively altering the power applied to silicon target, with no substrate external heating.

Figure 1 shows the RBS spectrum for sample $Zr_{0.920}Si_{0.080}N$. Polyethylene substrate was used for RBS analyses in order to allow the quantitative analyses of light chemical elements, such as nitrogen and oxygen. Similar spectra (not shown) were obtained for the other Zr-Si-N samples.

Some chemical elements can be identified at Figure 1: zirconium, silicon and nitrogen (originated from the thin film), carbon (from polyethylene substrate), hafnium (an inherent contamination from Zr target) and oxygen (originated from unavoidable O_2 and H_2O present in deposition chamber). Hf and O concentrations did not exceed 1 and 3 at. %, respectively and, for practical effects, only chemical elements related to the thin films (Zr, Si and N) will be considered in this work. Table 1 presents chemical composition of selected samples.

Pure ZrN sample presents near stoichiometric concentration, confirming the correct deposition parameters choice for ZrN and Zr-Si-N thin films evaluated in the present work. Two Zr-Si-N samples were selected based on RBS results: 1.6 at. % Si and 8.0 at. % Si, samples $Zr_{0.984}Si_{0.016}N$ and $Zr_{0.920}Si_{0.080}N$, respectively.

In succession to determination of deposition parameters, new samples were deposited on silicon substrates: substrate at room temperature (RT) and heated at 973 K during deposition. These samples were used for GAXRD, SEM-FEG, XPS and nanohardness analyses.

3.2. GAXRD

Figure 2 shows GAXRD patterns of zirconium silicon nitride thin films with 1.6 at. % Si deposited at room temperature (sample $Zr_{0.984}Si_{0.016}N$_RT) and heated to 973 K (sample $Zr_{0.984}Si_{0.016}N$_973). Both samples presented diffraction peaks corresponding to crystalline planes (111), (200), (220) and (311), characteristic from ZrN B1-NaCl crystalline phase (PDF 35-753). X-ray diffraction peaks referring to silicon phases could not be identified.

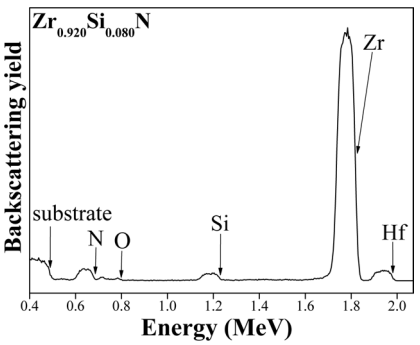

Figure 1. RBS analysis for sample $Zr_{0.920}Si_{0.080}N$.

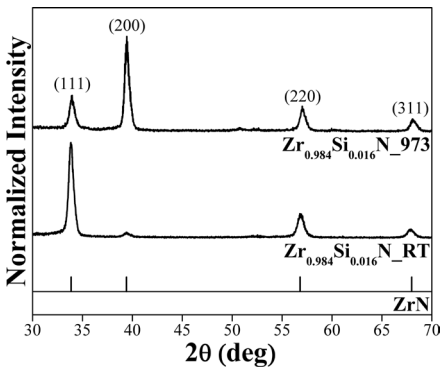

Figure 2. GAXRD patterns of $Zr_{0.984}Si_{0.016}N$_RT and $Zr_{0.984}Si_{0.016}N$_973.

Table 1. Chemical composition of samples ZrN, $Zr_{0.984}Si_{0.016}N$ and $Zr_{0.920}Si_{0.080}N$ obtained through RBS analysis.

	Si (at.%)	Zr (at.%)	N (at.%)
$Zr_{0.920}Si_{0.080}N$	8.0 ± 0.5	38.6 ± 0.9	53.4 ± 0.8
$Zr_{0.984}Si_{0.016}N$	1.6 ± 0.6	45.9 ± 0.5	52.5 ± 0.8
ZrN		50.1 ± 0.6	49.9 ± 0.9

A variation in thin films XRD patterns is clearly observed. The preferential plane orientation shifts from (111) to (200) as a direct consequence of applied substrate heating during the deposition.

Preferential (111) growth has the lowest deformation energy, since it allows the accommodation of a greater number of defects. Under these conditions, the structure will arrange itself in order to reduce thin film residual tension, contributing to strain energy reduction.

On the other hand, substrate heating promotes greater atoms mobility in the thin film, promoting preferential (200) growth, since this plane has the lowest surface energy and is more compact when compared to (111) grains.

The shift of (111) plane growth to (200) due to substrate temperature has already been reported in earlier works for pure ZrN and for other nitrides as well[12-14], therefore, it is not possible to attribute this event to Si incorporation in the coatings, but rather to the higher atom mobility during the thin film process formation, as a result of high substrate temperature during deposition.

Furthermore, upon deeper comparison of both samples, there are no XRD peaks shifting to lower or higher angles regions, and no evidence of substitutional or interstitial solid solution formation with Si, despite of substrate heating.

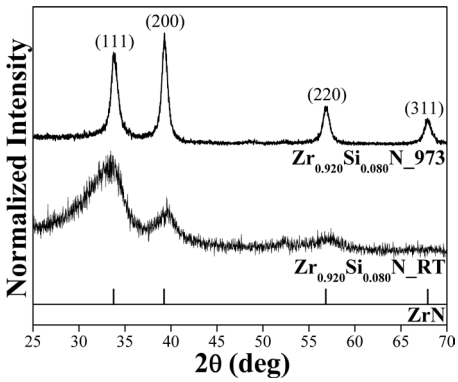

Figure 3. GAXRD patterns of $Zr_{0.920}Si_{0.080}N\_RT$ and $Zr_{0.920}Si_{0.080}N\_973$.

Figure 3 shows the GAXRD patterns for samples $Zr_{0.920}Si_{0.080}N\_RT$ and $Zr_{0.920}Si_{0.080}N\_973$. The amorphous characteristics presented for $Zr_{0.920}Si_{0.080}N\_RT$ are evident, however, it is still possible to identify broad peaks with low intensity in ZrN patterns peak positions. The crystallinity loss can be attributed to Si_3N_4 amorphous phase formation, which distort the ZrN crystalline lattice. This behavior was also reported in previous works[9,15].

Similarly to samples with 1.6 at. % Si, it was not possible to observe the formation of new compounds due to substrate heating. Previously identified ZrN peaks are present in sample $Zr_{0.920}Si_{0.080}N\_973$ and substrate heating is responsible only for the increase in thin film crystallinity.

Given $Zr_{0.920}Si_{0.080}N\_RT$ has shown an amorphous behavior, it was not possible to evaluate diffraction peaks shifting between the samples, however, comparing $Zr_{0.920}Si_{0.080}N\_973$ peaks position with the results obtained from Zr-Si-N samples with 1.6 at. % Si, shown in Figure 2, there were no peaks shifts for lower or higher angles among the three thin films. Again, by GAXRD analyses, there is no evidence that silicon is present in solid solution in $Zr_{0.920}Si_{0.080}N\_973$, despite substrate heating applied during deposition.

3.3. SEM-FEG

Figures 4a and 4b show cross-section images of $Zr_{0.984}Si_{0.016}N\_RT$ and $Zr_{0.984}Si_{0.016}N\_973$ performed by SEM-FEG. Both samples presenting columnar growth in their structures, a behavior commonly observed in thin films deposited by PVD techniques, however, this phenomenon is explicitly more pronounced for sample $Zr_{0.984}Si_{0.016}N\_973$.

Based on Structure Zone Model (SZM) proposed by Thornton[16,17], samples $Zr_{0.984}Si_{0.016}N\_RT$ and $Zr_{0.984}Si_{0.016}N\_973$ exhibit a transition from Zone T to Zone 2, respectively, evidenced by the change from a columnar structure with flat surface (Figure 4a) to wider and denser columns, in addition to the irregular feature on top of the coating (Figure 4b).

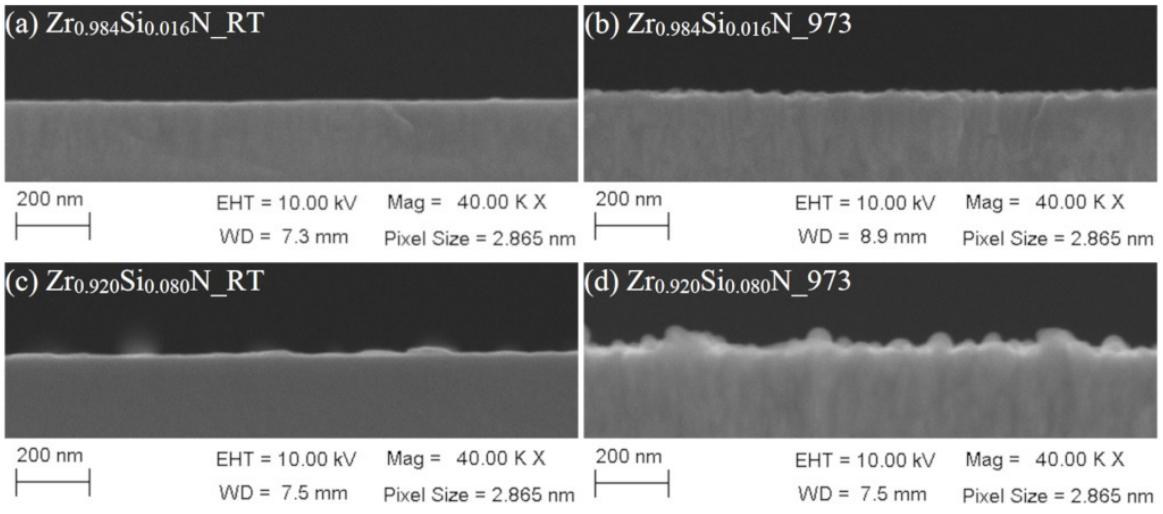

Figure 4. Cross-section SEM-FEG images of (a) $Zr_{0.984}Si_{0.016}N\_RT$, (b) $Zr_{0.984}Si_{0.016}N\_973$, (c) $Zr_{0.920}Si_{0.080}N\_RT$ and (d) $Zr_{0.920}Si_{0.080}N\_973$.

In Structure Zone Model is considered the argon discharge pressure, substrate temperature (T_{sub}) and material melting point (T_m) to categorized thin film structure in four different zones: Zone 1 (Z1 - limited surface diffusion of adatoms and amorphous crystallographic structure), Zone T (ZT - thermally enhanced surface diffusion, poorly defined columns and flat topography), Zone 2 (Z2 - higher surface diffusion, well-defined columns and high crystallinity) and Zone 3 (Z3 - dominating bulk diffusion process and denser columns).

SEM/FEG analyses of $Zr_{0.920}Si_{0.080}N\_RT$ is shown in Figure 4c. Differently to samples with 1.6 at. % Si, this sample has a smoother and more uniform appearance, showing no columnar growth evidence, with the thin film morphology identified as Zone 1 in SZM. This behavior occurs probably due to the presence of Si_3N_4 amorphous clusters, resulting in the ZrN columnar structure elimination.

Figure 4d shows cross-section images of $Zr_{0.920}Si_{0.080}N\_973$. It is possible to identify similar columnar growth as observed in Figure 4a and 4b and identified as Zone 2 in the SZM. Furthermore, heating the substrate clearly suppresses the amorphous behavior found in sample $Zr_{0.920}Si_{0.080}N\_RT$ and promotes gains in crystallinity, as shown in GAXRD results in Figure 3.

It is noteworthy that samples with substrate heating, showed in Figures 4b and 4d, are at the same Zone (Z2), but with distinct morphological characteristics, which suggests different regions positions on the model. The sample $Zr_{0.984}Si_{0.016}N\_973$ seems to be at the very beginning of Z2, presenting a combined of Z1 and Z2 characteristics, whereas $Zr_{0.920}Si_{0.080}N\_973$ is properly at Z2 and clearly manifests its features, displaying projection of clusters beyond the surface.

No previous works regarding Zr-Si-N deposited at high temperature can be found with similar results than the observed for sample $Zr_{0.920}Si_{0.080}N\_973$. An explanation for this phenomenon may be related to nitride decomposition, leading to N_2 diffusion to the surface and resulting in a rough appearance. Nevertheless, this argument must be corroborated with a more specific characterization technique, such as XPS.

3.4. XPS

Figure 5 shows the Si 2p photoelectronic region for samples $Zr_{0.984}Si_{0.016}N\_RT$ and $Zr_{0.984}Si_{0.016}N\_973$. Only one silicon surface species can be identified occurring at binding energy of 101.7 eV for Si $2p_{3/2}$ electronic level, associated with the compound Si_3N_4. No SiO_2 compound (103.2 eV)[18,19] or Si-Zr bonds (98.6 eV)[20,21] can be identified at Si 2p photoelectron region analyses.

Substrate external heating during deposition did not substantially modify the XPS Si 2p region analyses, except for the shift in Si binding energy value. This variation has been previously reported in literature, the binding energy for Si can be found between 100.5 eV to 102.0 eV, depending on the deposition parameters used[8,22].

Through these analyses, it was not possible to observe presence of silicon atoms in interstitial or substitucional solid solution in ZrN matrix. Such fact demonstrates that silicon, when added in 1.6 at. % in zirconium silicon nitride thin films, remains as Si_3N_4 amorphous phase even when it is heated to 973 K during deposition, corroborating to GAXRD results shown in Figure 2.

Figure 6 shows XPS results for samples $Zr_{0.920}Si_{0.080}N\_RT$ and $Zr_{0.920}Si_{0.080}N\_973$ to Si 2p spectrum. Similarly to analyses of zirconium silicon nitride with 1.6 at. % Si, Si 2p region components adjustment for both samples point to Si_3N_4 formation, suggesting that silicon atoms do not configure a solid solution in $Zr_{0.920}Si_{0.080}N\_973$.

However, $Zr_{0.920}Si_{0.080}N\_973$ presents a binding energy of 98.3 eV for Si $2p_{1/2}$ electronic level, attributed to Si-Si chemical bond, which could not be identified in the other samples. There is no evidence in literature regarding the presence of this component for zirconium silicon nitride thin films deposited at high temperature.

The Si-Si chemical bond presence may be related to Si_3N_4 decomposition into nitrogen and silicon when subjected to 973 K during deposition. XPS analyses confirm the possibility that the surface clusters presented in the SEM-FEG micrograph shown in Figure 4d may, indeed, be originated from Si_3N_4 amorphous phase dissociation, with nitrogen diffusing to the surface as N_2 and increasing the surface roughness.

In order to verify whether ZrN decomposition also occurred, in addition to that observed for Si_3N_4, Zr 3d photoelectronic region for $Zr_{0.920}Si_{0.080}N\_973$ is shown in Figure 7.

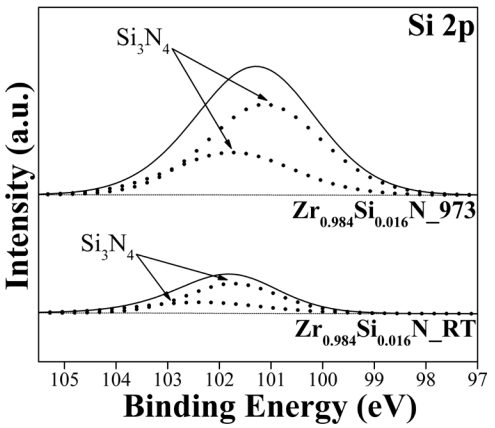

Figure 5. Si 2p XPS spectrum of $Zr_{0.984}Si_{0.016}N\_RT$ and $Zr_{0.984}Si_{0.016}N\_973$.

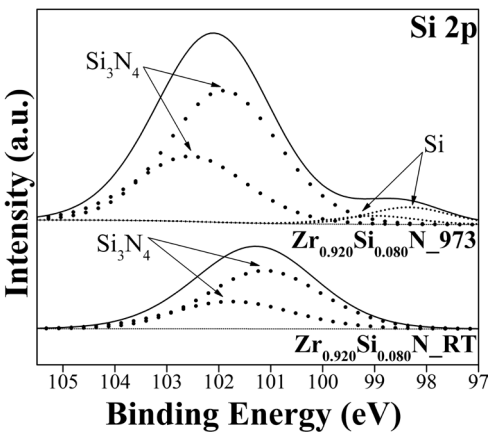

Figure 6. Si 2p XPS spectrum of $Zr_{0.920}Si_{0.080}N\_RT$ and $Zr_{0.920}Si_{0.080}N\_973$.

Table 2. Hardness values of all samples obtained through nanohardness tests.

Samples	Hardness values (GPa)
$Zr_{0.984}Si_{0.016}N\_RT$	25.1 ± 1.2
$Zr_{0.984}Si_{0.016}N\_973$	33.3 ± 1.6
$Zr_{0.920}Si_{0.080}N\_RT$	21.3 ± 1.1
$Zr_{0.920}Si_{0.080}N\_973$	25.0 ± 1.2

The envelope of Zr 3d region has three doublets identified, with binding energies of 179.8 eV, 181.6 eV and 182.5 eV for Zr $3d_{5/2}$ electronic level associated with the compounds ZrN, ZrO_x and ZrO_2, respectively, in agreement with values found in literature[5,23-25].

Differently than silicon, Zr 3d electronic level analyses for $Zr_{0.920}Si_{0.080}N\_973$ do not show Zr-Zr chemical bond, which should be present at the binding energy equal to 178.8 eV[18,26]. The zirconium atoms are present only as zirconium nitride or zirconium oxide. Since ZrN is much more stable than silicon nitride, with the Gibbs free energy of formation values equal to -120 Kcal/mol and -50 Kcal/mol at 973 K[27], respectively, it is very likely that only the Si_3N_4 amorphous phase decomposed, with ZrN grains remaining unaltered due to substrate external heating.

The chemical dissociation observed for Si_3N_4 possibly occurred only in a small portion of this phase, since XPS analyses still exhibit peaks related to silicon nitride. Moreover, this phenomenon does not occur in $Zr_{0.984}Si_{0.016}N\_973$ despite if this sample presenting Si_3N_4 amorphous phase, possibly due to Si_3N_4 being present as nanoclusters, a much more stable structure than the coarse grains present in $Zr_{0.920}Si_{0.080}N\_973$.

3.5. Nanohardness

Table 2 shows nanohardness tests results for all deposited samples. $Zr_{0.984}Si_{0.016}N\_RT$ and $Zr_{0.984}Si_{0.016}N\_973$ present hardness values of 25.1 GPa and 33.3 GPa, respectively.

The increase in hardness between the two samples cannot be directly correlated to substrate heating during deposition. It most likely occurs due to the modification in preferential plane orientation from (111) to (200), as observed in GAXRD analyses, once crystalline plan (200) is more compact than (111).

$Zr_{0.920}Si_{0.080}N\_RT$ and $Zr_{0.920}Si_{0.080}N\_973$ presented hardness of 21.3 and 25.0 GPa, respectively. It is not possible to discern the hardness between the two samples since both values are within the measurement error margin, moreover, hardness values are similar to the sample $Zr_{0.984}Si_{0.016}N\_RT$.

The hardness value obtained for $Zr_{0.920}Si_{0.080}N\_973$ cannot be directly correlated to silicon structural modification in the thin film. It is most likely a result of two factors: (a) silicon nitride phase dissolution in $Si+N_2$ observed in the SEM-FEG and XPS analyses, generating defects on thin film structure and (b) similar intensities of crystalline phases (111) and (200), as seen in Figure 3, with the absence of preferential phase (200) observed in $Zr_{0.984}Si_{0.016}N\_973$ sample, justifying the hardness perpetuation when compared to sample $Zr_{0.920}Si_{0.080}N\_RT$.

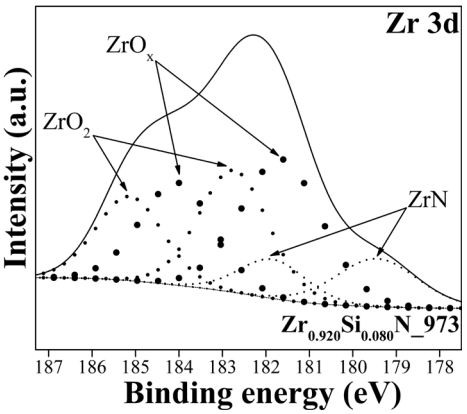

Figure 7. Zr 3d XPS spectrum of $Zr_{0.920}Si_{0.080}N\_973$.

4. Conclusions

Zirconium silicon nitride thin films with 1.6 and 8.0 at. % Si addition were successfully deposited at room temperature and 973 K. Through GAXRD analyses it was not possible to identify formation of new compounds, nor ZrN peaks shift. SEM-FEG analysis shows $Zr_{0.920}Si_{0.080}N\_973$ sample exhibited a different behavior from others, showing greater roughness and surface clusters, which occurred due to Si_3N_4 decomposition. This phenomenon was corroborated by XPS analyses, which revealed elemental Si in $Zr_{0.920}Si_{0.080}N\_973$ structure. Nanohardness analyses of samples with 1.6 at. % Si showed 30% increase due to modification on preferential plane orientation, however, this did not occur for sample with 8.0 at. % Si. This sample had its hardness values unaltered due to Si_3N_4 phase decomposition and the presence of (111) and (200) grains orientation in the same intensity. Through characterizations discussed in this work, it was proven the non-formation of solid solution in Zr-Si-N thin films, regardless of silicon amount and substrate heating during deposition.

5. Acknowledgments

The authors want to thank the UFRGS Ionic Implantation Laboratory for RBS analyses and CENANO-INT-RJ for XPS analyses. This work was supported by CAPES, CNPQ, and FAPITEC/SE.

6. References

1. Saladukhin I, Abadias G, Uglov V, Zlotski S, Michel A, Janse van Vuuren A. Thermal stability and oxidation resistance of ZrSiN nanocomposite and ZrN/ SiNX multilayered coatings: a comparative study. Surf Coat Tech. 2017;332:428-39.
2. Zhou M, Nose M, Deguchi Y, Mae T, Nogi K. Influence of sputtering conditions on microstructure and mechanical properties of Zr-Si-N films prepared by radio- frequency-reactive sputtering. J Vac Sci Technol A. 2003;21(5):1791-5.
3. Mae T, Nose M, Zhou M, Nagae T, Shimamura K. The effects of Si addition on the structure and mechanical properties of ZrN thin films deposited by an r.f. reactive sputtering method. Surf Coat Tech. 2001;142-144:954-8.
4. Nose M, Chiou W, Zhou M, Mae T, Meshii M. Microstructure and mechanical properties of Zr-Si-N films prepared by rf-reactive sputtering. J Vac Sci Technol A. 2002;20(3):823-8.

5. Choi N, Jang J, Zhang T, Kim J, Park I, Kim K. Effect of Si addition on the microstructure, mechanical properties and tribological properties of Zr-Si-N nanocomposite coatings deposited by a hybrid coating system. Surf Coat Tech. 2014;259:707-13.
6. Dong Y, Zhao W, Li Y, Li G. Influence of silicon on the microstructure and mechanical properties of Zr–Si–N composite films. Appl Surf Sci. 2006;252(14):5057-62.
7. Yalamanchili K, Jiménez-Piqué E, Pelcastre L, Bakoglidis K, Roa J, Johansson Jöesaar M. Influence of microstructure and mechanical properties on the tribological behavior of reactive arc deposited Zr-Si-N coatings at room and high temperature. Surf Coat Tech. 2016;304:393-400.
8. Dias IL, Terto AR, Silva PC No, Ramirez DA, Tentardini EK. Structural investigation of ZrN+Si_3N_4 thin films co-deposited by magnetron sputtering. Surf Eng. 2022;38(7-9):761-8.
9. Yalamanchili K, Forsén R, Jiménez-Piqué E, Johansson Jöesaar M, Roa J, Ghafoor N, et al. Structure, deformation and fracture of arc evaporated Zr–Si–N hard films. Surf Coat Tech. 2014;258:1100-7.
10. Pilloud D, Pierson J, Marco de Lucas M, Alnot M. Stabilisation of tetragonal zirconia in oxidized Zr-Si-N nanocomposite coatings. Appl Surf Sci. 2004;229(1-4):132-9.
11. Sandu CS, Medjani F, Sanjinés R, Karimi A, Lévy F. Structure, morphology and electrical properties of sputtered Zr–Si–N thin films: from solid solution to nanocomposite. Surf Coat Tech. 2006;201(7):4219-23.
12. Roman D, Bernardi JC, Boeira CD, Souza FS, Spinelli A, Figueroa CA, et al. Nanomechanical and electrochemical properties of ZrN coated NiTi shape memory alloy. Surf Coat Tech. 2012;206(22):4645-50.
13. Kumar K, Singh D, Kumar R, Kaur D. Effect of crystallographic orientation of nanocrystalline TiN on structural, electrical and mechanical properties of TiN/NiTi thin films. J Alloys Compd. 2009;479(1-2):166-72.
14. Portolan E, Amorim CLC, Soares GV, Aguzzoli C, Perottoni CA, Baumvol IJR, et al. Carbon occupancy of interstitial sites in vanadium carbide films deposited by direct current reactive magnetron sputtering. Thin Solid Films. 2009;517(24):6493-6.
15. Tang Q, Wu Y, Lou B, Chen Z, Lee J. Mechanical property evaluation of ZrSiN films deposited by a hybrid superimposed high power impulse- medium frequency sputtering and RF sputtering system. Surf Coat Tech. 2019;376:59-67.
16. Thornton JA. High rate thick film growth. Annu Rev Mater Sci. 1977;7(1):239-60.
17. Kusano E. Structure-zone modeling of sputter-deposited thin films: a brief review. Appl Sci Converg Technol. 2019;28(6):179-85.
18. Yamauchi T, Kitamura H, Wakai N, Zaima S, Koide Y, Yasuda Y. Photoelectron spectroscopic studies on interfacial reactions in Zr/ 2x1 (100) Si and Zr/ SiO2/ 9 (100) Si System. J Vac Sci Technol. 1993;2619:6493-6.
19. Bois L, L'Haridon P, Laurent Y, Gouin X, Grange P, Létard J-F, et al. Characterization of a boro-silicon oxynitride prepared by thermal nitridation of a polyborosiloxane. J Alloys Compd. 1996;232(1-2):244-53.
20. Liu W, Liang J, Zhou X, Long X. Formation of zirconium silicide between silicon substrate and zirconium films. Mater Lett. 2014;122:220-2.
21. Zhu D, Huang Z, Shi M, Qin Y, Zou Z, Deng Z. High char yield BPR modified with ZrSi2 and B4C: pyrolysis kinetic behavior and structure evolution. J Therm Anal Calorim. 2023;148(3):789-805.
22. Zhang G, Niu E, Wang X, Lv G, Zhou L, Pang H, et al. Characterization of Zr–Si–N films deposited by cathodic vacuum arc with different N_2/SiH_4 flow rates. Appl Surf Sci. 2012;258(8):3674-8.
23. Chang L, Zheng Y, Chen Y, Chang S, Liu B. Bonding characteristics and chemical inertness of Zr–Si–N coatings with a high Si content in glass molding. Coatings. 2018;8(5):181.
24. Nishino Y, Krauss A, Lin Y, Gruen D. Initial oxidation of zirconium and Zircaloy-2 with oxygen and water vapor at room temperature. J Nucl Mater. 1996;228(3):346-53.
25. Baba Y, Sasaki T, Takano I. Preparation of nitride films by Ar+ion bombardment of metals in nitrogen atmosphere. J Vac Sci Technol A. 1988;6(5):2945-8.
26. Takano L, Isobe S, Sasaki TA, Baba Y. Nitrogenation of various transition metals by N + 2- ion implantation. Appl Surf Sci. 1989;37(1):25-32.
27. Reed TB. Free energy of formation of binary compounds: an atlas of charts for high-temperature chemical calculations. Cambridge: MIT Press; 1971.